Solvation of Coumarin 153 in Supercritical Fluoroform

Francesca Ingrosso,*,†,‡ Branka M. Ladanyi,†,§ Benedetta Mennucci,‡ and Giovanni Scalmani[||]

Department of Chemistry, Colorado State University, Fort Collins, Colorado 80523, Dipartimento di Chimica e Chimica Industriale, Università di Pisa, Via Risorgimento 35, 56126 Pisa, Italy, and Gaussian Inc., 340 Quinnipiac St, Building 40, Wallingford, Connecticut 06492

Received: October 28, 2005; In Final Form: January 12, 2006

We present a study of local density augmentation around an attractive solute (i.e., giving rise to more attractive interaction with the solvent than solvent−solvent interactions) in supercritical fluoroform. This work is based on molecular dynamics simulations of coumarin 153 in supercritical fluoroform at densities both above and below the critical density, ranging from dilute gaslike to liquidlike, at a reduced temperature (T/T_c) of 1.03. We focused on studying the structure of the solvation shell and the variation of the solute electronic absorption and emission shifts with density. Quantum calculations at the density functional theory (DFT) level were run on the solute in the ground state, and time-dependent DFT calculations were performed in the solute excited state in order to determine the solute−solvent potential parameters. The results obtained for the Stokes shift are in agreement with the experimental measurements. To evaluate local density augmentation from simulations, we used two different definitions, one based on the solvation number and the other derived from solvatochromic shifts. In the former case, the agreement with experimental results is good, while, in the latter case, better agreement is achieved by perturbatively including the induced-dipole contribution to the solvation energy.

1. Introduction

One of the major applications of supercritical fluids (SCFs) is to use them as solvents, since they represent an environmentally safe alternative to some commonly employed organic liquids.[1,2] Due to the possibility of continuously changing the density of supercritical fluids from dilute gaslike to liquidlike by changing the pressure, reaction conditions can usually be controlled and monitored. The interest of experimental and theoretical investigations in this field in the past 20 years has therefore focused on understanding and modeling the interactions which play an important role in supercritical solutions and their dependence on solvent density.

Local density inhomogeneities are one of the characteristics of the supercritical regime.[3,4] Density fluctuations become larger and larger when approaching the critical point, and the divergence of the compressibility of the fluid at the critical point can be related to a divergence in the correlation length. This means that density fluctuations extend to a macroscopic scale.

To avoid such large fluctuation at the critical point, most experimental and computational studies are addressed to the "near-critical" region, in which local density inhomogeneities are still present but macroscopic effects are avoided. This is usually accomplished by working at a temperature slightly higher than the critical temperature. From now on, we will refer to such conditions when mentioning the supercritical phase.

Additional inhomogeneities in the near-critical region are induced by the presence of a solute. In fact, the presence of a solute can give rise to local density inhomogeneities which are related to the strength of the attraction between the solute and the solvent. The most studied solutes are the so-called attractive[3,4] ones, because they produce a local density augmentation (LDA) effect. This effect often manifests itself as a "three-regime" behavior:[3,5] as the bulk density increases from $\rho = 0$, the local density first rapidly increases and then reaches a plateau after which it becomes proportional to ρ. The presence of the plateau is related to smaller changes in local density with respect to what is expected from bulk density variations, and it is an indication of solvent clustering around the solute.

Local density augmentation is not directly measurable experimentally, but it can be deduced from the density dependence of vibrational or electronic spectral features.

Analyses based on the Kamlet−Taft[6] and the $E_T(30)$[7] polarity scales were carried out[8−10] to study local density augmentation on the basis of solvatochromic shifts of the solute.

Polarity scales establish a connection between the energy variation of the solute electronic transition and electrostatic solute−solvent interactions. In the first case, the solvent polarity is classified on the basis of the effect it has on the $\pi \rightarrow \pi^*$ transition of a probe solute and a parameter describing the effect of the solvent on the solute transition is extrapolated from experimental spectra in solution. The $E_T(30)$ polarity scale is analogously related to the effect of solvent polarity on the $S_0 \rightarrow S_1$ electronic transition energy of the polar probe betaine-30.

Measured electronic spectra of solute probes in supercritical solvents at different densities have been analyzed[8−10] by making use of these polarity scales. The parameters extrapolated in both cases, which are a measure of solute−solvent interactions, were plotted as a function of density. The curve thus obtained showed the characteristic shape of the three-regime behavior. Augmentation effects were also studied on the basis of the solvent effect on charge transfer electronic excited states of the solute.[11,12]

Using fluorescence spectroscopy data, Maroncelli and collaborators characterized the effect of LDA on the solvent

* Corresponding author. Present address: Colorado State University. E-mail: fingross@gmail.com.
† Colorado State University.
‡ Università di Pisa.
§ Corresponding author. E-mail: bl@lamar.colostate.edu.
|| Gaussian Inc.

10.1021/jp056226b CCC: $33.50
Published on Web 02/14/2006

reorganization energy, finding that it is mainly due to the interaction between the solute dipole and the charge distribution of the solvent.[13] In the same paper, they also defined a consistent procedure to extract effective local densities from solvatochromic shifts. Investigations[14] based on measurements on a larger number of solute−solvent systems led to the conclusion that there is a correlation between LDA and the solvation free energy.

From a theoretical point of view, computer simulations have been employed to describe solutions in the supercritical regime (see ref 3 for a review). In particular, calculations of solvation energies and solvatochromic shifts of electronic spectra have been performed in recent simulation-based studies.[14−21]

Giving a correct description of electrostatic interactions in polar SCFs is the main interest of recent theoretical work, since indeed solvatochromic shifts in polar SCFs and LDA effects are related to solute−solvent interactions. Our work represents a further contribution to the interpretation of these effects and is based on molecular dynamics simulations of coumarin 153 (C153) in supercritical fluoroform.

Our goal is to study solute−solvent interactions in the supercritical regime through the analysis of LDA effects and of the solvation shell changes with bulk density. We have performed simulations at 10 different densities both above and below the critical one, for C153 in the ground state and in the excited state. The solute is described at atomistic level, and its structure and its partial charges, both in the ground state and in the excited state, were obtained from quantum mechanical calculations. The model for the solvent is a nonpolarizable, two-site model[22] which has been optimized to reproduce the main properties of CHF_3 for values of the reduced density ($\rho_r = \rho/\rho_c$, with ρ_c being the critical density) between 0.1 and 2.0.

To avoid the large fluctuations in the proximity of the critical point, we worked at a temperature slightly higher than the critical one. The same procedure is also adopted in conducting experiments. Local density augmentation is evaluated from the distribution of solvent molecules in the first solvation shell and from the density dependence of line shifts of absorption and emission spectra of C153. In the latter case, we show with a simple model, based on first-order perturbation theory, that the inclusion of the interaction of the solute with solvent induced dipoles represents an important step in the description of solvation in the supercritical regime. Solute−solvent orientational correlations are calculated as well, to gain more insight into the structure of the first solvation shell.

This paper is organized as follows. Section 2 summarizes the theoretical concepts used in this work. In particular, after presenting in section 2.1 the theoretical background for the calculation of the Stokes shifts and for the contributions to them from induced-dipole interactions, the definition of local density augmentation is given and discussed in section 2.2, while section 2.3 treats orientational correlations.

The details about the computational procedures, the quantum calculations on C153 and the molecular dynamics simulations in SC fluoroform, are described in section 3. Section 4 includes a presentation of our results and a discussion based on comparison with experimental data. Section 5 is devoted to conclusions.

2. Theoretical Background

2.1. Steady-State Stokes Shift. The solvatochromic shift in a polar solvent can be defined in terms of the difference in the solute Hamiltonian between the excited state and the ground state:

$$H_{exc} - H_{gr} = h\nu_0 + \Delta E \tag{1}$$

where ΔE represents the difference in the intermolecular potential for the solute in the excited state and the ground state. The shift in the absorption ($\Delta\nu_{abs}$) can be calculated as an average of ΔE in an equilibrium simulation in the ground state (referred to as 0), while the emission shift ($\Delta\nu_{em}$) has the same definition on the basis of an equilibrium simulation in an excited state (referred to as 1):

$$h\Delta\nu_{abs(em)} = \langle \Delta E \rangle_{0(1)} \tag{2}$$

After converting the energy into frequency, the steady-state Stokes shift is calculated as the difference between the absorption and emission shifts:[21,23,24]

$$\Delta\Delta\nu = \Delta\nu_{abs} - \Delta\nu_{em} \tag{3}$$

If the main contribution to the solute−solvent intermolecular potential is the electrostatic (elec) interaction, ΔE in eq 1 can be evaluated according to[21,24]

$$\Delta E \approx \Delta E_{elec} = \frac{1}{4\pi\epsilon_0} \sum_{j=1}^{N_{solv}} \sum_{\gamma \in sol} \sum_{\eta \in solv} \frac{\Delta q_\gamma q_{j\eta}}{r_{\gamma,j\eta}} \tag{4}$$

where the sum over j runs over N_{solv} solvent molecules, γ is a solute site, and η is a solvent site. The difference (Δq_γ) is calculated between the partial charge on the solute site (γ) in the excited state and in the ground state, while $q_{j\eta}$ is the partial charge of site η in solvent molecule j.

A description based on electrostatic interactions only could fail for systems in which effects related to the polarizability of molecules are not negligible. Even though in the system that we are studying (a polar solute giving rise to dipolar excitation in a polar solvent) the electrostatic portion is likely the major term, we propose a way to evaluate the effects related to the interaction between the solute charge distribution and the dipoles induced on the solvent molecules.

At a first level of approximation, we can estimate the magnitude of this term with a simple electrostatic model in which we neglect the mutual polarization between solute and solvent by using first-order perturbation theory.

We described the effect of the polarization on each solvent molecule j as being due to the presence of an electric field, $\mathbf{e}_j$, generated by the solute, which gives rise to an induced dipole, $\boldsymbol{\mu}_{ind,j}$. The first-order perturbation to the total interaction energy can be written as the difference between the contributions in the excited (1) and ground (0) states as

$$\Delta E_{ind} = E_{ind}^{(1)} - E_{ind}^{(0)} \tag{5}$$

where

$$E_{ind}^{(n)} = \sum_{j=1}^{N_{solv}} - \boldsymbol{\mu}_{ind,j}^{(n)} \cdot \mathbf{e}_j^{(n)} \tag{6}$$

and the sum is extended to the total number of solvent molecules (N_{solv}) in the simulation.

The induced dipole can be expressed in terms of the molecular polarizability tensor ($\boldsymbol{\alpha}_j$) of molecule j in the laboratory frame

as $\boldsymbol{\mu}_{\mathrm{ind},j} = \boldsymbol{\alpha}_j \cdot \mathbf{e}_j$, while the electric field ($\mathbf{e}_j$) is a function of the charge distribution on the solute sites ($\mathbf{q}$):

$$\mathbf{e}_j^{(n)} = -\frac{1}{4\pi\epsilon_0}\sum_{\gamma\in\mathrm{sol}} q_\gamma^{(n)} \nabla_\gamma\left(\frac{1}{r_{\gamma j}}\right) = -\mathbf{q}^{(n)}\cdot\mathbf{G}_j \qquad (7)$$

where $r_{\gamma j}$ is the distance between the solute site (γ) and the center of mass of solvent molecule j and where we defined a matrix, $\mathbf{G}_j$, the dimensions of which are $N_{\mathrm{sol}} \times 3$ and the γ, j elements of which are $\mathbf{G}_{\gamma j} = (1/4\pi\epsilon_0)\nabla_\gamma(1/r_{\gamma j})$.

We finally obtain for the first-order perturbation term in eq 5

$$\Delta E_{\mathrm{ind}} = -\sum_{j=1}^{N_{\mathrm{solv}}} \{(\mathbf{q}^{(1)}\cdot\mathbf{G}_j)\cdot\boldsymbol{\alpha}_j\cdot(\mathbf{q}^{(1)}\cdot\mathbf{G}_j) - (\mathbf{q}^{(0)}\cdot\mathbf{G}_j)\cdot\boldsymbol{\alpha}_j\cdot(\mathbf{q}^{(0)}\cdot\mathbf{G}_j)\} \qquad (8)$$

The calculation of the fluoroform gas-phase molecular polarizability tensor was performed with the Gaussian program.[25] Calculations were run with the Møller−Plesset correlation energy correction method truncated at the second order,[26] with an augmented Dunning correlation consistent basis set (aug-cc-pVDZ)[27] and preceded by geometry optimization at the same level. The values that we obtained in the molecular frame (M) are $\alpha_{xx}^M = \alpha_{yy}^M = 2.75$ Å^3 and $\alpha_{zz}^M = 2.47$ Å^3 (the z axis is the molecular symmetry axis). The isotropic value of the polarizability is therefore 2.67 Å^3, in good agreement with the experimental value 2.8 Å^3.[28]

Section 4.1 contains the results that we have obtained for the steady-state Stokes shifts.

2.2. Local Density Augmentation. The characterization of density augmentation in supercritical fluids is based on the evaluation of the effective density (ρ_{eff}) that is experienced by a target molecule. Since we are interested in solvation, the natural choice is represented by the solute. Experimental results[23] are available for the system of interest: coumarin 153 in SC fluoroform.

We used two different ways for evaluating the effective local density, both being related to properties that can be obtained from simulations. One definition is based on the number of solvent molecules in the first solvation shell, while the other is related to estimates of the solvatochromic shift of either absorption or emission frequency of the solute electronic spectra. The latter represents the way in which experimental evaluation of LDA is often provided.

Let us first introduce the definition based on the solvation number (N). In previous works,[3,21] the solvation number has been calculated as the result of the integral

$$N_{\mathrm{com}}(R;\rho) = 4\pi\rho\int_0^R g_{\mathrm{sS}}(r) r^2\, \mathrm{d}r \qquad (9)$$

of the solute−solvent-center-of-mass (com) radial distribution function extended to a length, R, equal to the position of the first minimum of $g_{\mathrm{sS}}(r)$. In the case of C153, which has an almost planar geometry giving rise to a highly nonspherical distribution of solvent molecules (see, for example, ref 16 for a description of solvent density around planar solutes in supercritical solvents), this definition cannot be applied. The procedure that we adopted is described below, and it is based on the methodology described in ref 16.

First of all, the maximum radius within which a solvent molecule is considered part of the first solvation shell was defined. We therefore calculated solute−solvent site-center-of-mass distribution functions, and from these functions, we evaluated the first minimum position (R) and averaged the values of R over all solute sites. The position of the minimum varied from 3.8 to 5.0 Å for the H atoms, which are more external with respect to the molecular structure, to 6.8−7.7 Å for the C atoms in the aromatic rings. We found that there is negligible variation of the R value with the bulk density. On the other hand R has a slightly different value in the ground state ($R = 5.38$ Å) and in the excited state ($R = 5.33$ Å). Since we are interested in variations in LDA around the solute in the ground state and in the excited state, we used the value $R = 5.38$ Å as a reference for both states. The solvation number was then calculated as the average number of solvent molecules within R from at least one C153 site.

To stress that the solvation number that we evaluated is obtained in a different way with respect to eq 9, from now on, we use a different subscript, N_{sites}.

From solvation numbers obtained at different densities, it is possible to calculate the effective density (ρ_{eff}) in terms of a reference liquidlike density (ρ_{ref}) as[16]

$$\rho_{\mathrm{eff}}(\rho) = \rho_{\mathrm{ref}}\frac{N_{\mathrm{sites}}(R;\rho)}{N_{\mathrm{sites}}(R;\rho_{\mathrm{ref}})} \qquad (10)$$

We emphasize here that such a definition is based on the evaluation of the distance R to define the solvation shell.

As was done in ref 23, we set $\rho_{\mathrm{r}} = 2.0$ as a reference density. Augmentation data will generally be presented and discussed in terms of the reduced density (ρ_{r}), which is the most common way in which experimental data are reported.

The reduced density augmentation is defined as

$$\Delta\rho_{\mathrm{eff,r}}(\rho_{\mathrm{r}}) = \frac{\Delta\rho_{\mathrm{eff}}(\rho_{\mathrm{r}})}{\rho_{\mathrm{c}}} = \frac{\rho_{\mathrm{eff}}(\rho_{\mathrm{r}}) - \rho}{\rho_{\mathrm{c}}} \qquad (11)$$

and it is characterized by the presence of a maximum usually located in the range $\rho_{\mathrm{r}} = 0.5-0.6$.[3,4]

As already mentioned, the effective density (ρ_{eff}) can be defined in terms of the observed (absorption, emission) line shifts ($\Delta\nu_{\mathrm{obsd}}$). These shifts can be either measured or calculated from simulation, as described in section 2.1.

We assume that continuum dielectric theory gives an estimate of the solvent shifts in the absence of local density augmentation. Such estimates are possible according to the expression[23]

$$\Delta\nu(\rho_{\mathrm{r}}) = \gamma R(n^2) + \zeta R(\epsilon) \qquad (12)$$

where the variables which depend on the reduced density are n, the solvent refractive index, and ϵ, the static dielectric constant. The function R is defined as

$$R(x) = \frac{x-1}{x+2} \qquad (13)$$

The functions $n^2(\rho_{\mathrm{r}})$ and $\epsilon(\rho_{\mathrm{r}})$ were provided in ref 23, as results of fits to collected experimental measurements. We note that the first term in eq 12 is present only if induction is included in the solute−solvent interaction potential.

To determine the constants γ and ζ, we use the molecular dynamics (MD)-calculated shifts at the liquidlike density (assuming that enhancement due to augmentation in the SC regime is not present). This reduced density (equal to 2.0 ρ_{c}) is therefore assumed again as the reference (ref) density. Specif-

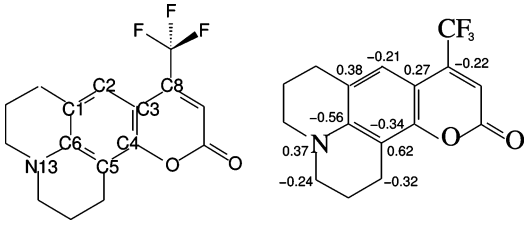

Figure 1. Coumarin 153. On the left side, labels used to identify the atomic sites of interest are shown. On the right side, excited-to-ground-state differences in the partial charges (atomic units) are displayed on the most representative sites of C153.

ically, in the absence of induction, when the shifts are calculated according to eq 4, we set

$$\Delta\nu_{\mathrm{elec,abs(em)}}(\rho_{\mathrm{ref}}) = \gamma_{\mathrm{abs(em)}} R[\epsilon(\rho_{\mathrm{ref}})] \tag{14}$$

obtaining the γ coefficient. When the contribution due to the induced-dipole interaction is considered (and calculated according to eq 8), we have

$$\Delta\nu_{\mathrm{ind,abs(em)}}(\rho_{\mathrm{ref}}) = \zeta_{\mathrm{abs(em)}} R[n^2(\rho_{\mathrm{ref}})] \tag{15}$$

which allows us to determine the ζ coefficient. In eqs 14 and 15, we used the value of ϵ calculated from simulation and the refractive index from experiments.[22] Eventually, the effective reduced density is calculated by inverting the relation $\Delta\nu = f(\rho_r)$; in particular, in the absence of induction, we invert the relation

$$\Delta\nu_{\mathrm{abs(em)}} = \gamma_{\mathrm{abs(em)}} R[\epsilon(\rho_{\mathrm{eff,r}})] \tag{16}$$

while, when induction is taken into account, we invert the general relation

$$\Delta\nu_{\mathrm{abs(em)}} = \gamma_{\mathrm{abs(em)}} R[\epsilon(\rho_{\mathrm{eff,r}})] + \zeta_{\mathrm{abs(em)}} R[n^2(\rho_{\mathrm{eff,r}})] \tag{17}$$

Section 4.2 reports the results that we obtained for the functions defined in eqs 10 and 11 by using both the definition of effective density based on the solvation number and the ones based on the line shifts of absorption and emission spectra, with a comparison with experiments.

2.3. Orientational Correlations. The importance of an analysis of solvation in SCFs based on a description of solute−solvent orientational correlations in the first solvation shells has been already pointed out.[21] In that paper, MD simulations in supercritical CO_2 showed changes in solute−solvent pair correlations as a function of the density. In a polar fluid such as fluoroform, the most important contribution to solute−solvent correlations are the ones related to dipolar interactions.

The molecular pair distribution function of an isotropic fluid can be decomposed into a rotational invariant expansion.[29] The coefficients of the expansion are related to orientational correlations in the fluid. We are interested in solute−solvent orientational correlations, and we consider two internuclear axes in the C153 molecule, along the C3−C8 direction and the N13−C2 direction (see Figure 1 for labeling). These directions were chosen on the basis of the fact that they are good representatives of charge transfer (CT) occurring within the C153 molecule as a consequence of the transition of the excited state.[24] An additional reason for which the two chosen vectors are a good choice for describing CT is that the relative polarities of the two sites change between the ground and excited states: N13 and C3 become more positive, while C2 and C8 become more negative (see Figure 1 and relative discussion), following the electron flux from the donor (amino group) to the acceptor (CF_3 group).

By analogy with solvent−solvent correlations, we therefore defined one unit vector, $\hat{u}_1$, along the distance between two solute sites, one along the solvent dipole moment, $\hat{u}_2$, and the third one, $\hat{r}_{12}$, along the distance between the solvent center of mass and the midpoint between the positions of the solute atoms considered.

The pair correlations depend on the three vectors defined above, which characterize the indices (m, n, l) of the coefficients $h^{mnl}(r)$ in the rotational invariant expansion:[29]

$$h^{mnl}(r) = \frac{\int h(12)\Phi^{mnl}(12)\,\mathrm{d}\Omega_1\,\mathrm{d}\Omega_2}{\int [\Phi^{mnl}(12)]^2\,\mathrm{d}\Omega_1\,\mathrm{d}\Omega_2} \tag{18}$$

where $h(12) = g(12) - 1$ is the total pair correlation between molecules 1 and 2, $\Phi^{mnl}(12)$ is a rotational invariant function, while Ω_1 and Ω_2 are solid angles describing molecular orientations. The simple form of eq 18, in which only three indices describe solute−solvent orientation, is due to the fact that we consider only individual unit vectors along two particular internuclear distances in the C153 molecule.

The rotational invariant ($\Phi^{110}(12)$) depends on intermolecular dipolar correlation, being related to the mutual orientation of the molecules:

$$\Phi^{110}(12) = \hat{u}_1 \cdot \hat{u}_2 \tag{19}$$

The normalized function[30]

$$G_1(r) = \frac{h^{110}(r)}{3g^{000}(r)} = \overline{\cos\theta_{12}} \tag{20}$$

is the average cosine angle ($\cos\theta_{12}$) between vectors $\hat{u}_1$ and $\hat{u}_2$ whose centers are at a distance r, and g^{000} ($g^{000} = h^{000} + 1$) is the spherically symmetric projection of the pair distribution $g(12)$.

The rotational invariant ($\Phi^{112}(12)$) has the symmetry of a dipole−dipole interaction and is given by the following expression:

$$\Phi^{112}(12) = 3(\hat{u}_1 \cdot \hat{r}_{12})(\hat{u}_2 \cdot \hat{r}_{12}) - \hat{u}_1 \cdot \hat{u}_2 \tag{21}$$

We show and analyze the results that we have obtained for solute−solvent orientational correlations in section 4.2 and discuss them on the basis of the changes in the local density.

3. Computational Details

Simulations of C153 in two-site fluoroform[22] at different densities in the proximity of the critical density (two-site model $\rho_c = 0.541$ g/cm^3,[22] experimental $\rho_c = 0.526$ g/cm^3 [31]) were performed in the microcanonical ensamble using a modified version of DL_POLY_2.[32] We chose 10 different densities, ranging from $\rho_r = 0.13$ (dilute gas-phase-like) to $\rho_r = 2.0$ (liquidlike), and the number of solvent molecules in the cubic simulation box was increased from 255 to 499 for the higher densities in order to avoid size effects. At densities corresponding to 0.59 ρ_c and 0.95 ρ_c, size effects were checked by performing simulations with the 255 and 499 solvent molecule systems, from which solvatochromic shifts were calculated and compared. The simulation error bars on the shifts were the same (200 cm^{-1}) in both cases, and the average values agreed within the error bars.

Simulations were run at a temperature which is slightly higher than the critical one ($T/T_c \simeq 1.03$). The critical temperature for the model used is $T_c = 300.2$ K (experimental $T_c = 299.1$ K[31]). At densities close to the critical value, the simulated temperature fluctuated the most, and the average value was slightly smaller (i.e., at $\rho_r = 0.95$, we had $T = 307 \pm 8$ K). Similar behavior was found for the lower, gas-phase-like density, while, for example, we had $T = 310 \pm 4$ K for the liquidlike density.

The model used for the solvent was rigid and nonpolarizable,[22] while some of the intramolecular motions in the solute molecule were taken into account.[24]

The constraints for the solvent and for the nonflexible part of the solute structure were kept rigid by using the SHAKE[33] algorithm. The integration of the equation of motion was performed according to the Verlet leapfrog algorithm,[34] and the long-range interactions were calculated using the Ewald method with conducting boundary conditions. The intermolecular potential used in the simulations was a combination of Coulombic and Lennard-Jones (LJ) terms:

$$u_{mn}(r) = 4\epsilon_{mn}\left[\left(\frac{\sigma_{mn}}{r}\right)^{12} - \left(\frac{\sigma_{mn}}{r}\right)^{6}\right] + \frac{q_m q_n}{4\pi\epsilon_0 r} \qquad (22)$$

where m and n are two sites on two different molecules and the parameters σ and ϵ are associated with the well depth and the diameter of the LJ potential. The Lennard-Jones parameters for fluoroform provided in ref 22 were employed, while for C153 we made use of the parameters in ref 35. The Lorentz−Berthelot combining rules[34] were used to define the LJ parameters for unlike pairs of atoms:

$$\epsilon_{mn} = \sqrt{\epsilon_m \epsilon_n} \qquad (23)$$

$$\sigma_{mn} = \frac{\sigma_m + \sigma_n}{2} \qquad (24)$$

The LJ potential at each density was cut off at half the simulation box length.

We performed equilibrium simulations of ground- and excited-state C153 for each density. The time step employed in all simulations was 2 fs. At the higher densities considered, an equilibration of 2 ns and trajectories run for 2 ns were sufficient to obtain reasonably averaged properties. On the other hand, at those densities at which the effects of augmentation are higher ($\rho_r \leq 0.95$), a longer equilibration time (3−4 ns) and a longer acquisition time (4 ns) were necessary.

As for the solute, geometries and partial charges for the ground state in a vacuum were obtained by using the Gaussian 03 package.[25] Geometry optimization of the ground state was obtained by employing the density functional theory (DFT) with the hybrid B3LYP exchange-correlation functional[36] based on the LYP functional by Lee, Parr, and Yang.[37] The basis set used in the calculation was of the Dunning−Huzinaga full-double-ζ type,[38] with the inclusion of polarization and diffuse functions (D95++(d,p)), while the basis set used for geometry optimization was a 6-311G type[39] with inclusion of the d polarization functions (6-311G(d)).

The characteristics of the ground-state geometry were in agreement with previous studies performed at the DFT level;[40] in particular, we found that the lower energy conformation is the one corresponding to a syn arrangement of the unsaturated rings with respect to the N13 atom. The ground-state dipole moment was 7.7 D (based on the use of a different functional; in ref 40, Cave and Castner found 7.24 D, while Muhlpfordt et al.[41] found 8.1 D). However, measurements of the ground-state dipole moment[42] provide a slightly smaller value (6.5 D). To obtain parameters for the solute which can describe electrostatic interactions as close to experiments as possible, we used the partial charges obtained in ref 24 with a Hartree−Fock (HF) calculation, since the latter provided a value of 6.9 D for the ground-state dipole moment, in better agreement with experiment. Ground-state partial charges were therefore obtained by using the CHelp scheme,[43] based on fitting the electrostatic potential from the HF calculation on the nuclei positions.

A development version of Gaussian[44] was employed for obtaining accurate partial charges for C153 in the first electronic excited state. A time-dependent density functional theory (TD-DFT) calculation of the excited-state relaxed density matrix was run by employing the same basis set and the same functional used for the ground state. This calculation has been made possible by the recent implementation in Gaussian of the analytical gradients for TD-DFT energies.[45]

The excited-state dipole moment that we obtained was 13.4 D. The excited-to-ground-state difference in the dipole moment is therefore about 6.4 D, which lies within the interval defined by different experimental measurements[46−49] (between 4.9 and 9 D). In particular, a very accurate value was provided by recent measurements in the gas phase,[50] which corresponds to a change of 7.1 D.

Partial charges were obtained in an analogous way to the one used for the ground state. We report in Figure 1 the values of the charge difference between the excited state and the ground state on the coumarin sites for which such a variation is the largest.

The centers which are more affected by the excitation are those lying between the donor (amino group) and the acceptor ($-CF_3$ group), and the polarity of the variation along the N13−O and C1−C8 directions and within the left aromatic ring changes between adjacent sites, leading to an overall flux of negative charge toward $-CF_3$.

As in ref 24, excited-state geometry was obtained through optimization with the configuration interaction of all single excitations[51] (CIS) method and a 6-311G(d) basis set. As can be expected on the basis of the fairly rigid structure of the molecule, very small changes are observed between the excited-state and ground-state geometries.

For three different density values ($\rho_r = 0.13$, 0.59, and 2.0) in the interval considered, we ran simulations by using solute geometries and partial charges in the presence of a continuum, polarizable solvent by means of the integral equation formulation of the polarizable continuum model (IEFPCM)[52,53] implemented in Gaussian 03. The calculation level and the basis set were the same as described above for the vacuum calculations (details about the molecular cavity employed can be found in ref 24). Values of the dielectric constant corresponding to the solvent density and temperature considered were employed in the simulation: we used here the parametrization of collected experimental data provided in ref 13.

The simulations in the ground state and in the excited state were run under the same conditions described above; only the solute parameters were modified. As for the three densities considered, the results that we obtained for the properties we are interested in (LDA, orientational correlations, electronic shifts of absorption, and emission) were in all equivalent to the same results obtained by simulating a C153 molecule parametrized on the basis of quantum calculations in a vacuum. This is most likely due to the very small values of the dielectric constant of fluoroform in the density interval under study and to the particular solute considered: almost no variation of either

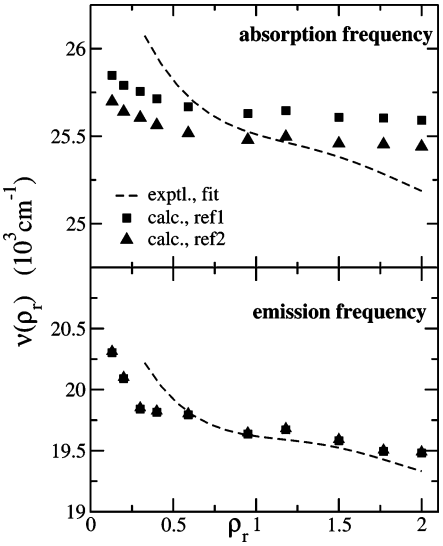

Figure 2. Calculated frequency for the electronic absorption (top panel) and emission (bottom panel) processes compared to experimental results from ref 23 (fit, dashed line). Two different reference solvents are used to calculate the frequency from the calculated shift (see text): 2-methylbutane (full squares) and cyclohexane (full triangles).

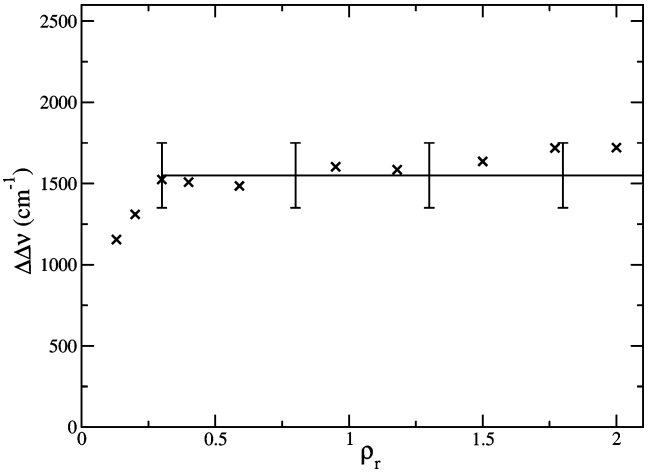

Figure 3. Steady-state Stokes shifts of C153 in supercritical fluoroform as a function of the reduced density (crosses), compared to the experimental result in ref 23. Experimental data are reported as an average value with uncertainty (full line).

ground- or excited-state geometry with ϵ was observed, and negligible differences were observed in the charge distribution. We used this result to simplify our simulations and employ the parameters obtained in vacuo in the whole density interval considered. The results reported in the next section refer to simulations with such parameters for C153.

4. Results

4.1. Solvatochromic Shifts. In this section, we present the results that we obtained for electronic absorption and emission line shifts, using eq 2, and for the steady-state Stokes shift, according to eq 3, and discuss them on the basis of experimental results available in the literature[23] in the interval between $\rho_r = 0.3$ and $\rho_r = 2.1$. We are aware of other measurements[54,55] of solvatochromism for the system of interest. However, ref 23 contains a detailed description of LDA from line shifts and it is therefore more suitable for a comparison with our calculated results.

Results are collected in Figures 2 and 3. To compare our results to experimental measurements of absorption and emission frequency as a function of the reduced density, we had to calculate the absolute variation of the frequency by adding the corresponding $\nu^{ref}_{abs,em}$ values measured in a nonpolar solvent:[56]

$$\nu_{abs(em)} = \Delta\nu_{abs(em)} + \nu^{ref}_{abs(em)} \qquad (25)$$

We used two different solvents as the references, such as 2-methylbutane (ref 1) and cyclohexane (ref 2). The absorption frequencies for C153 were 26 130 and 25 980 cm^{-1}, while the emission frequencies were 21 740 and 21 750 cm^{-1}, respectively.

Let us first discuss the absorption and emission results. In the top panel of Figure 2, absorption data are collected. The agreement between simulation and experiment is qualitatively good, but discrepancies in the density dependence of the absorption frequency are observed especially in the low and high density regions. The calculated results appear to be less dependent on density variations than the experimental ones. The same observations can be applied to the emission shifts reported in the bottom panel of Figure 2, even though they are in better agreement with experiment. Our absorption frequency values are more strongly affected by the different choices of reference solvent than are the emission frequencies.

Let us turn to the Stokes shift results displayed in Figure 3. Very weak density dependence is observed and data can be considered constant within the experimental error,[23] in the density interval considered. This observation is well reproduced by simulated data, at densities for which the experimental data were available (i.e., $\rho_r > 0.3$) We notice that the comparison between experiment and calculation in this case is more straightforward than in the case of line shifts of absorption and emission, from which we had to extrapolate the density dependence of the frequency before comparing them with experimental results.

Calculated data reasonably reproduce not only the density dependence of the Stokes shift but also the magnitude of the shifts, which is in agreement with experiments.

Even though the reason for the behavior of the Stokes shift as a function of the density is still not clear, we observe that this result is connected to the absorption and emission line shifts having a similar deviation from linearity at all densities. We recall that the Stokes shift has been shown to be related to the solvent reorganization energy.[3] The experimental result in the SC region seems to suggest that the energy used by the solvent to move from the perturbed configuration right after excitation of the solute to a new equilibrium configuration is not strongly influenced by changes in the local density. This result might be characteristic of this particular system, in which strong polar solute−solvent interactions are present. However, experimental results for a solute subject to much smaller changes during electronic excitation with respect to C153, such as 9-cyanoanthracene, confirmed the very weak density dependence of the Stokes shift.[13] In addition, results[21] from simulations in a nondipolar solvent such as SC CO_2 provided a further example of negligible density dependence of the Stokes shift for solutes immersed in SC solvents.

4.2. Local Density Augmentation. In this section, results for the effective local density and for the density augmentation are presented.

We start the discussion of LDA by showing the solute-site−solvent-center-of-mass pair correlation functions for some significant coumarin sites at three different densities, namely,

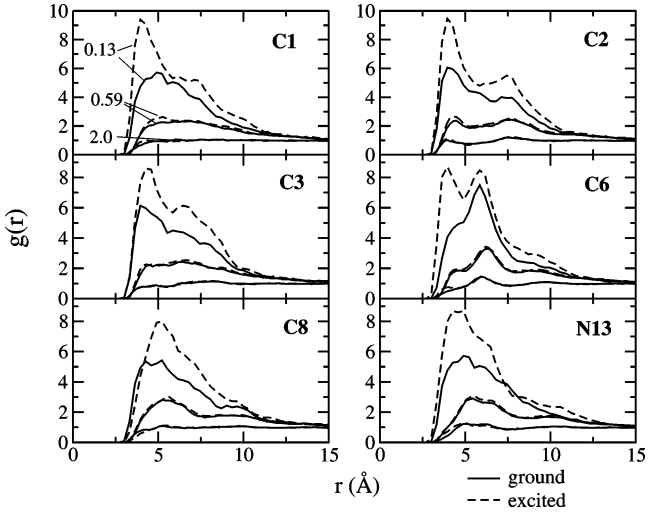

Figure 4. Solute−solvent pair correlation functions for some of the coumarin sites at three different densities, as indicated in the top left panel.

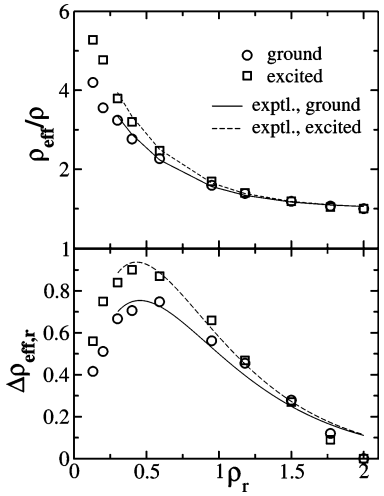

Figure 5. Local density augmentation: results calculated from the solvation number (see eq 10) are shown as open circles for the ground state and as open squares for the excited state. The experimental results from ref 23 are presented as fitted curves (ground state, full line; excited state, dashed line).

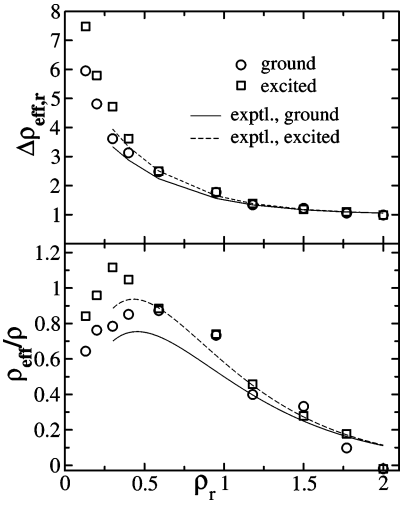

Figure 6. Local density augmentation: results calculated from the electronic shifts (inversion of eq 16) are shown as open circles for the ground state and as open squares for the excited state. As in Figure 5, experimental results[23] are presented as fitted curves.

the lowest one considered in our simulations, an intermediate one, and the liquidlike one, as shown in Figure 4. In the figure, we reported results from equilibrium simulations in the ground state and in the excited state. There are two main observations which can be made on the basis of these results. One concerns the observed difference between the excited-state and ground-state results, and the other concerns the density dependence of such a difference.

We notice that the functions calculated for the low density show a relatively large change in augmentation around the C153 sites when the solute undergoes electronic excitation. This is consistent with a more attractive interaction potential in the excited state and a higher value of the molecular dipole moment. In some cases, even the shape of the pair correlation function at distances corresponding to the first solvation shell changes (see for example atom C6).

However, as for those functions calculated at intermediate and high densities, the enhancement associated with electronic transition becomes smaller and smaller. When looking at results in the same scale, as in Figure 4, in the latter cases, the ground- and excited-state results are almost superimposed, and much smaller differences in the shape of the functions, especially at distances corresponding to the first two solvation shells, are seen.

When the density increases, the overall number of molecules which can fit in each solvation shell tends to become similar, due to saturation effects, which applies both to the ground state and to the excited state,[57] and therefore, visualizing the effects of augmentation on the basis of the pair correlation functions becomes more difficult. On the other hand, when the density dependence of the solvation number is studied to calculate the effective density, as defined in eq 10, differences between clustering in the ground state and in the excited state become more evident, as we shall show in the following discussion.

Let us now introduce the results obtained for local density augmentation. Equations 10−17 were used in order to compare our results with experimental data in the interval between $\rho_r = 0.3$ and $\rho_r = 2.0$. In ref 23, experimental data for ρ_{eff}/ρ are presented as a function of the reduced density (ρ_r) as fits to the expression

$$\frac{\rho_{eff}(\rho_r)}{\rho} = 1 + Be^{-C\rho_r} \tag{26}$$

$\Delta\rho_{eff,r}(\rho_r)$ is usually well fitted by a Weibull function:[13,14,21,23]

$$\Delta\rho_{eff,r}(\rho_r) = a\chi^{-\chi}\left[\frac{\rho_r - \rho_0}{\beta} + \chi^{1/c}\right]^{c-1} \times \exp\left\{-\left[\frac{\rho_r - \rho_0}{\beta} + \chi^{1/c}\right]^{c} + \chi\right\}, \quad \chi = \frac{c-1}{c} \tag{27}$$

Figures 5 and 6 present collected results of density augmentation, from our calculations and from experimental measurements.[23] We recall here that the latter are evaluated on the basis of treatment of measured shifts of absorption and emission spectra, while, in the case of the calculated results from simulations, we made use of two different definitions of the effective density, one based on the evaluation of the solvation number (as in eq 10) and the other based on the evaluation of electronic line shifts (as in eqs 16 and 17). The results for the former are shown in Figure 5, while those for the latter are shown in Figures 6 and 7.

Starting from Figure 5, we see that in this case the agreement between calculation and experiment for both ρ_{eff}/ρ and $\Delta\rho_{eff,r}$

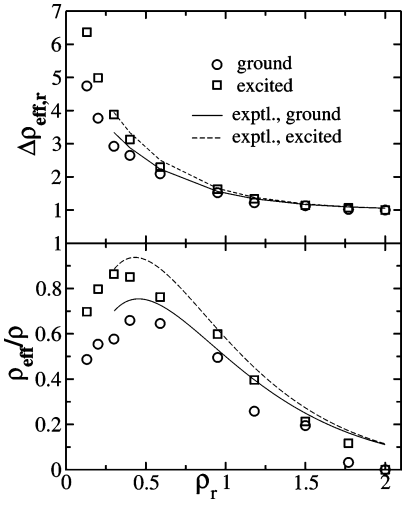

Figure 7. Local density augmentation data, presented as in Figure 6. Results from effective density calculated by inverting eq 17, which includes a contribution from induction, are shown.

is good. The small discrepancies for $\Delta\rho_{eff,r}$ at high values of the reduced density depend on the way in which the calculation was performed, since by definition this function is zero at $\rho_r = 2.0$. For the same function, the ground-state result from simulation seems to peak at a slightly large value of the reduced density. Nonetheless, the width and the height of the curve reproduced are in good accord with experiment.

The results shown in Figure 6 refer to inversion of eq 16, which does not take into account the induction. Augmentation effects seem systematically overestimated, but the maximum position and the width of the curves reasonably reproduce the experimental results. Even though the overall value that we obtained for the Stokes shift is correct, it seems that the density dependence of the solvatochromic shifts presents discrepancies with respect to experimental data, which propagate to the evaluation of LDA.

We recall here that solvation shifts calculated with our nonpolarizable model do not take into account induction effects given in eq 8. The difference with experimental data could therefore be due to the neglect of the contribution to the solute−solvent interaction generated by the solute charge distribution polarizing the solvent. We incorporated the term due to the induced-dipole effect (eq 8) and calculated the effective reduced density by inverting eq 17. The results are shown in Figure 7. We notice an improvement with respect to the results in Figure 6, which stresses the importance of induction contributions to the solvation energy in the SC phase.

Tables 1 and 2 collect the parameters obtained by fitting our data with the fit functions in eqs 26 and 27, respectively, compared to the experimental ones.

4.3. Orientational Correlations. The focus of the following discussion will be in analyzing solute−solvent configurations in the first solvation shell by means of orientational correlations. As already discussed, the directions C3 → C8 and N13 → C2 (see Figure 1) represent the flux of charge from the donor (amino-) group to the acceptor ($-CF_3$) in the charge transfer electronic transition that we are considering. We therefore calculated solute−solvent orientational correlations involving these two vectors.

We consider first dipolar orientational correlations. Figure 8 displays a 3D visualization of the results that we obtained for the h^{110} function (see eqs 18 and 19) for the densities considered. For both for C3−C8 and N13−C2 directions, orientational correlations are stronger in the excited state than in the ground

TABLE 1: Calculated and Experimental[23] Parameters for the Fitting Function in eq 26

simulation[a]	S_0	S_1
B	4.0	6.8
C	2.05	2.37
simulation[b]	S_0	S_1
B	6.7	9.3
C	2.8	3.1
simulation[c]	S_0	S_1
B	5.1	7.8
C	2.8	3.2
experiment	S_0	S_1
B	4.51	5.91
C	2.20	2.32

[a] Equation 10. [b] Equation 16. [c] Equation 17.

TABLE 2: Calculated and Experimental[23] Parameters for the Fitting Function in eq 27

simulation[a]	S_0	S_1
α	0.75	0.92
β	0.95	0.89
c	1.77	1.7
ρ_0	0.56	0.49
simulation[b]	S_0	S_1
a	0.87	1.01
β	1.33	0.84
c	2.4	1.5
ρ_0	0.54	0.37
simulation[c]	S_0	S_1
α	0.66	0.85
β	1.15	1.02
c	2.3	1.8
ρ_0	0.51	0.41
experiment	S_0	S_1
α	0.750	0.996
β	1.885	1.414
c	3.254	2.236
ρ_0	0.564	0.490

[a] Equation 10. [b] Equation 16. [c] Equation 17.

state and larger values for the first peaks are associated with the C3−C8 direction. The charge differences q(C8) − q(C3) and q(C2) − q(N13) are both positive in the ground state and negative in the excited state, as a consequence of the charge transfer from the amino group to the $-CF_3$ group of the coumarin.

The $S_0 \rightarrow S_1$ excitation changes the mutual orientation between the solvent and these two directions toward a predominately antiparallel alignment at distances corresponding to the first solvation shell. The effects become more and more evident at lower densities, as is typical of the SC regime.

The normalized $G_1(r)$ solute−solvent functions give more quantitative information about the average angle in the first solvation shell, according to eq 20. The average angle between the C3−C8 vector and the solvent dipole in the first solvation shell varies after electronic excitation from 71 to 149° (change in the orientation of 78°) at the lowest density, while the change is smaller (change of 34°), from 82 to 116°, at the highest density.

The changes in the N13−C2−solvent average angle after excitation vary between 52° for $\rho_r = 0.13$ (from 83 to 135°) and 35° for $\rho_r = 2.00$ (from 88 to 123°).

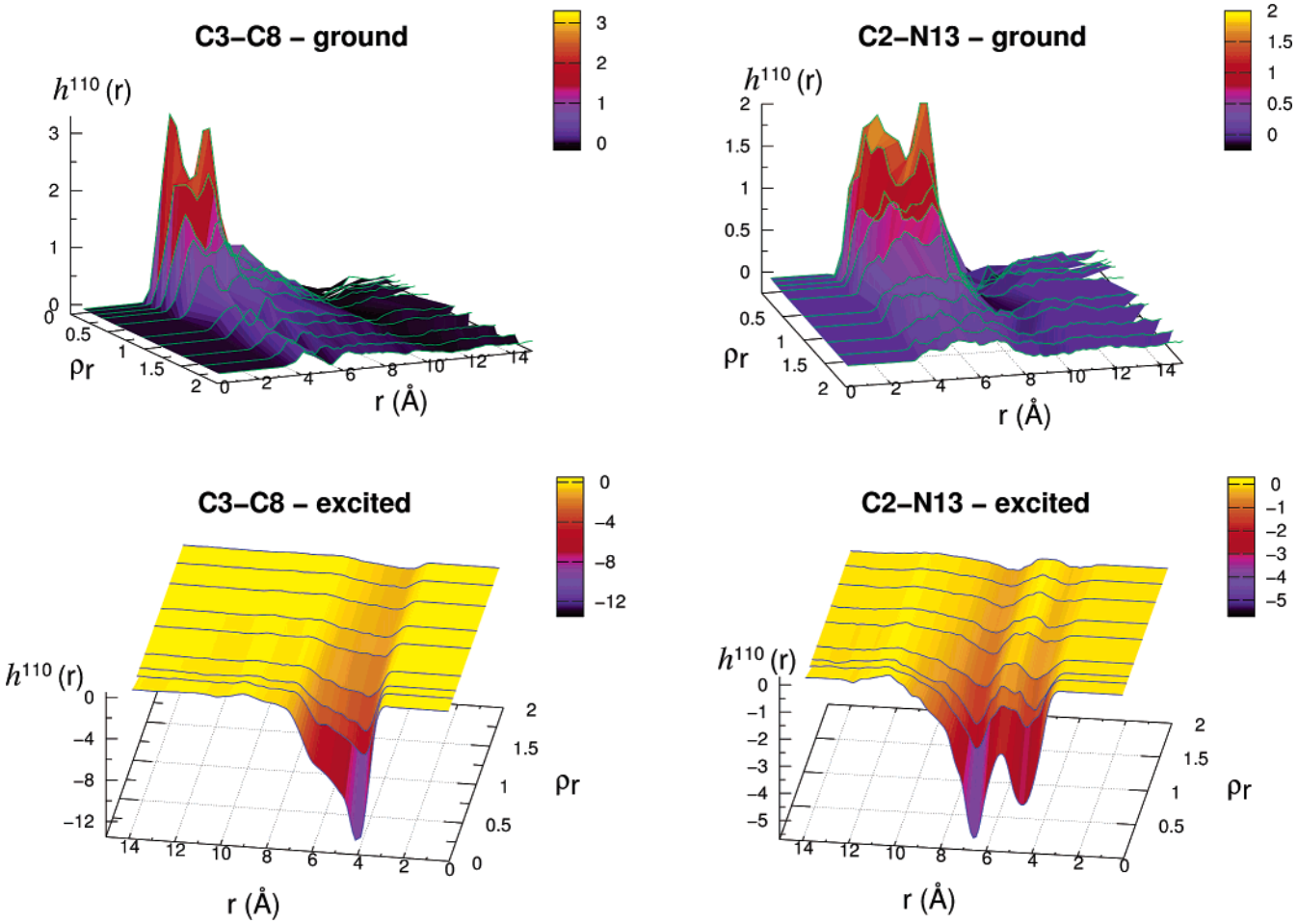

Figure 8. Solute−solvent orientational correlations as in eq 19 at the different densities considered in a 3D representation. The solute internuclear vector is along the C3−C8 direction (left side) or along the N13−C2 direction (right side), while the top and bottom plots refer to simulations with the solute in the ground state and in the excited state, respectively.

This can be interpreted as a more pronounced tendency to antiparallel arrangement in the excited state, and larger effects are related to smaller values of the density, for which the reorientation of solvent molecules in the first solvation shell finds less impediment than at higher densities. The direction along which the changes with excitation are more pronounced is the C3−C8 one. This corresponds to a larger value of the charge difference between the two sites in the excited state (absolute difference of 0.5 au, against 0.3 au between N13 and C2), which possibly gives rise to slightly stronger electrostatic interactions with the solvent dipole.

A larger dipolar interaction in the excited state for the C3−C8 direction is confirmed by the calculation of the h^{112} function (see eq 21), as shown in Figure 9. Here, the excited-state functions have positive values corresponding to the first solvation shells (dipolar interactions are favorable for the antiparallel orientation) and vice versa in the ground state. We see that the ground-state values at all densities are comparable between the two directions, but the excited-state result shows a larger effect along the C3−C8 direction, confirming the result obtained in Figure 8.

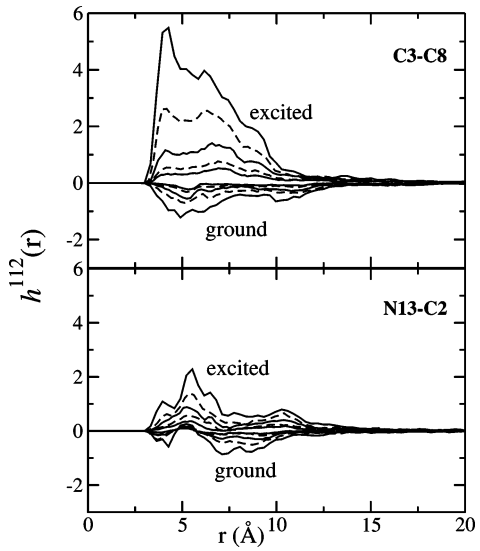

Figure 9. Solute−solvent correlations of dipolar symmetry (eq 21) at the reduced densities $\rho_r = 0.13$, 0.3, 0.59, 1.18, and 1.77. The positive (excited state) and negative (ground state) peak heights decrease with increasing density. The results for the solute internuclear vector along the C3−C8 direction are displayed in the top panel and for the vector along N13−C2 in the bottom panel.

5. Concluding Remarks

In this work, solute−solvent interactions in the supercritical regime were studied and analyzed in order to characterize local density augmentation effects and solvatochromism of a fluorescent probe by means of a two-site model for SC fluoroform and a molecular representation of the solute, C153.

When applied to the calculation of absorption and emission line shifts, our model was capable of providing results in agreement with available experimental data. Both the magnitude

and the density dependence of absorption and emission line shifts of C153 in the supercritical solvent showed agreement with the experimental measurements. In particular, very interesting is the confirmation of the experimental finding concerning the negligible changes in the Stokes shift of the solute $S_0 \rightarrow S_1$ electronic transition with the solvent bulk density. It therefore appears that the energy involved in the solvent reorganization process is not influenced by changes in the local density.

The line shifts can be used to define the effective density of solvent molecules around the solute. This quantity can also be evaluated from the simulation, on the basis of the calculation of the solvation number. Both definitions were applied to describe LDA and compare the results obtained with our model with the experimentally measured ones. According to this comparison, good results are obtained for the definition involving the solvation number. As for the definition based on the line shifts, we showed that the inclusion of the induced-dipole contribution in the solute−solvent interaction energy is necessary to improve the agreement with experiment. Further investigations of local density augmentation in the SC phase should therefore take into account polarizability effects, here evaluated with a very simple electrostatic model based on a first-order expansion of the interaction energy.

The information gained by studying orientational correlations helps one to picture the arrangement of solvent molecules around the solute at different densities. Variations of the average angle between the solute and surrounding solvent molecules were found in this work, corresponding to a larger tendency toward antiparallel alignment around the excited-state solute, as a consequence of the charge transfer from the donor to the acceptor group. Such a tendency leads to stronger dipolar interaction at lower densities.

This work represents part of a more general investigation of solvation in SC fluoroform. Further investigation will be devoted to time-dependent solvation properties and to a study of rotational and reorientational dynamics of the pure fluid. In addition, we are interested in including molecular polarizabilities in the intermolecular interaction potential. This can be accomplished by employing polarizable intermolecular potentials.[58,59] Such a description indeed will provide an improved representation of the properties of the first solvation shell with the inclusion of the effects of interactions between induced dipoles that we showed to be non-negligible for C153 in SC fluoroform. Even more important is the possibility of applying this description to solutions in nonpolar solvents, in which induced-dipole contributions play a major role.

Acknowledgment. This work was supported by the NSF through grant CHE9981539 and the Italian MIUR. Financial support from Gaussian Inc. is also acknowledged. The authors are grateful to Prof. Mark Maroncelli and to Dr. Noritsugu Kometani for helpful discussions. In particular, we thank Prof. Maroncelli for carefully reading the manuscript and providing us with his comments and suggestions.

References and Notes

(1) Eckert, C. A.; Knutson, B. L.; Debenedetti, P. G. *Nature* **1996**, *383*, 313.

(2) Sunol, A. K.; Sunol, S. S. Handbook of solvents. In *Substitution of solvents by safer products and processes*; Wypych, G., Ed.; William Andrew and Chem Tec publishing: Toronto and New York, 2001.

(3) Tucker, S. C. *Chem. Rev.* **1999**, *99*, 391.

(4) Kajimoto, O. *Chem. Rev.* **1999**, *99*, 355.

(5) Brennecke, J. F.; Chateauneuf, J. E. *Chem. Rev.* **1999**, *99*, 433.

(6) Kamlet, M. J.; Abboud, J. L.; Taft, R. W. *J. Am. Chem. Soc.* **1977**, *99*, 8325.

(7) Dimroth, K.; Reichardt, C.; Siepmann, T.; Bohlmann, F. *Liebigs Ann. Chem* **1963**, *661*, 1.

(8) Smith, R. D.; Frye, S. L.; Yonker, C. R.; Gale, R. W. *J. Phys. Chem.* **1987**, *91*, 3059.

(9) Sigman, M. E.; Lindley, S. M.; Leffker, J. E. *J. Am. Chem. Soc.* **1985**, *107*, 1471.

(10) Kim, S.; Johnston, K. P. *Ind. Eng. Chem. Res.* **1987**, *26*, 1206.

(11) Kajimoto, O.; Futakami, M.; Kobayashi, T.; Tamasaki, K. *J. Phys. Chem.* **1988**, *92*, 1347.

(12) Kometani, N.; Okamoto, J.; Asami, K.; Yonezawa, Y. *J. Phys.: Condens. Matter* **2002**, *14*, 114437.

(13) Lewis, J. E.; Biswas, R.; Robinson, A. G.; Maroncelli, M. *J. Phys. Chem. B* **2001**, *105*, 3306.

(14) Song, W.; Biswas, R.; Maroncelli, M. *J. Phys. Chem. A* **2000**, *104*, 6924.

(15) Luo, H.; Tucker, S. C. *Theor. Chem. Acc.* **1997**, *96*, 84.

(16) Patel, N.; Biswas, R.; Maroncelli, M. *J. Phys. Chem. B* **2002**, *106*, 7096.

(17) Adams, J. E. *J. Phys. Chem. B* **1998**, *102*, 7455.

(18) Egorov, S. A. *J. Chem. Phys.* **2000**, *113*, 1950.

(19) Egorov, S. A. *J. Chem. Phys.* **2002**, *116*, 2004.

(20) Egorov, S. A. *Phys. Rev. Lett.* **2004**, *93*, Art. No. 023004.

(21) Nugent, S.; Ladanyi, B. M. *J. Chem. Phys.* **2004**, *120*, 874.

(22) Song, W.; Patel, N.; Maroncelli, M. *J. Phys. Chem. B* **2002**, *106*, 8783.

(23) Biswas, R.; Lewis, J. E.; Maroncelli, M. *Chem. Phys. Lett.* **1999**, *310*, 485.

(24) Ingrosso, F.; Ladanyi, B. M.; Mennucci, B.; Elola, M. D.; Tomasi, J. *J. Phys. Chem. B* **2005**, *109*, 3553.

(25) Frisch, M. J.; et al. *Gaussian 2003*, revision B.03; Gaussian, Inc.: Pittsburgh, PA, 2003.

(26) Head-Gordon, M.; Pople, J. A.; Frisch, M. J. *Chem. Phys. Lett.* **1988**, *153*, 503.

(27) Woon, D. E.; Dunning, T. H., Jr. *J. Chem. Phys.* **1993**, *98*, 1358.

(28) Miller, C. K.; Orr, B. J.; Ward, J. F. *J. Chem. Phys.* **1981**, *74*, 4858.

(29) Stell, G.; Patey, G. N.; Høye, J. S. *Adv. Chem. Phys.* **1981**, *48*, 183.

(30) Edwards, D. M. F.; Madden, P. A.; McDonald, I. R. *Mol. Phys.* **1983**, *51*, 1141.

(31) Okazaki, S.; Matsumoto, M.; Okada, I.; Maeda, K.; Kataoka, Y. *J. Chem. Phys.* **1995**, *103*, 8594.

(32) Smith, W.; Forester, T. R. "DL_POLY_2", CCP5, Daresbury, Warrington, England, 1999.

(33) Ryckaert, J. P.; Ciccotti, G.; Berendsen, H. J. C. *J. Comput. Phys.* **1977**, *23*, 327.

(34) Allen, M. P.; Tildesley, D. J. *Computer simulation of liquids*; Oxford University Press: Oxford, U.K., 1987.

(35) Kumar, P. V.; Maroncelli, M. *J. Chem. Phys.* **1995**, *103*, 3038.

(36) Becke, A. *J. Chem. Phys.* **1993**, *98*, 5648.

(37) Lee, C.; Yang, W.; Parr, R. G. *Phys. Rev. B* **1988**, *37*, 785.

(38) Dunning, T. H.; Hay, P. J. In *Modern Theoretical Chemistry*; Schaefer, H. F., III, Ed.; Plenum: New York, 1976.

(39) McLean, A. D.; Chandler, G. S. *J. Chem. Phys.* **1980**, *72*, 5639.

(40) Cave, R. J.; Castner, W., Jr. *J. Phys Chem. A* **2002**, *106*, 12117.

(41) Mühlpfordt, A.; Schanz, R.; Ernsting, N. P.; Fartzinov, V.; Grimme, S. *Phys. Chem. Chem. Phys.* **1999**, *1*, 3209.

(42) Moylan, C. R. *J. Phys. Chem.* **1994**, *98*, 13513.

(43) Chirlian, L. E.; Francl, M. M. *J. Comput. Chem.* **1987**, *8*, 894.

(44) Frisch, M. J.; et al. *Gaussian Development Version*, revision D.01+; Gaussian, Inc.: Wallingford, CT, 2004.

(45) Scalmani, G.; Frisch, M. J.; Mennucci, B.; Tomasi, J.; Cammi, R.; Barone, V. *J. Chem. Phys.* **2006**, in press.

(46) Samanta, A.; Fessenden, R. W. *J. Phys. Chem. A* **2000**, *104*, 8577.

(47) Rechthaler, K.; Koehler, G. *Chem. Phys.* **1994**, *189*, 99.

(48) Smirnov, S. N.; Braun, C. L. *Rev. Sci. Instrum.* **1998**, *69*, 2875.

(49) Chowdhury, A.; Locknar, S. A.; Premvardhan, L. L.; Peteanu, L. A. *J. Phys. Chem. A* **1999**, *103*, 9614.

(50) Kanya, R.; Ohshima, Y. *Chem. Phys. Lett.* **2003**, *370*, 211.

(51) Foresman, J. B.; Head-Gordon, M.; Pople, J. A.; Frisch, M. J. *J. Phys. Chem.* **1992**, *96*, 135.

(52) Cancès, E.; Mennucci, B. *J. Math. Chem.* **1998**, *23*, 309.

(53) Mennucci, B.; Cancès, E.; Tomasi, J. *J. Chem. Phys.* **1998**, *109*, 249.

(54) Kimura, Y.; Hirota, N. *J. Chem. Phys.* **1999**, *111*, 5474.

(55) Takahashi, K.; Fujii, K.; Sawamura, S.; Jonah, S. D. *Radiat. Phys. Chem.* **1999**, *55*, 579.

(56) Horng, M. L.; Gardecki, J. A.; Papazyan, A.; Maroncelli, M. *J. Phys. Chem.* **1995**, *99*, 17311.

(57) Re, M.; Laria, D. *J. Phys. Chem. B* **1997**, *101*, 10494.

(58) Caldwell, J.; Dang, L. X.; Kollman, P. A. *J. Am. Chem. Soc.* **1990**, *112*, 9144.

(59) Yu, H.; Hannson, T.; van Gunsteren, W. F. *J. Chem. Phys.* **2003**, *118*, 221.